PHYSICAL REVIEW C VOLUME 16, NUMBER 4 OCTOBER 1977

(^{9}Be,^{8}Be) reaction at 50 MeV†

D. P. Stahel, G. J. Wozniak, M. S. Zisman, B. D. Jeltema,* and Joseph Cerny

Department of Chemistry and Lawrence Berkeley Laboratory, University of California, Berkeley, California 94720

(Received 14 June 1977)

The (^{9}Be,^{8}Be) reaction has been investigated at a bombarding energy of 50 MeV on targets of ^{12}C, ^{16}O, ^{26}Mg, ^{28}Si, ^{40}Ca, and ^{208}Pb. Owing to the small neutron binding energy of ^{9}Be and the resulting positive Q values, this reaction favors transitions involving small l transfers and populates states up to several MeV in excitation with a fairly high yield. In addition, a broad continuum in the energy spectra was observed that can be attributed to the breakup of the weakly bound ^{9}Be projectile. For the ^{28}Si, ^{40}Ca, and ^{208}Pb targets, spectroscopic factors have been extracted from exact finite-range distorted-wave Born-approximation calculations using optical-model potentials derived from ^{9}Be elastic-scattering data. The relative spectroscopic factors are in good agreement with those obtained from light-ion reactions but the absolute values are low.

[NUCLEAR REACTIONS ^{12}C, ^{16}O, ^{26}Mg, ^{28}Si, ^{40}Ca, ^{208}Pb (^{9}Be, ^{8}Be), ^{12}C, ^{28}Si, ^{40}Ca, ^{208}Pb (^{9}Be, ^{9}Be), E_{lab} = 50 MeV; measured $\sigma(E,\Theta)$ for ^{28}Si, ^{40}Ca, ^{208}Pb; optical model and EFR-DWBA analyses, deduced spectroscopic factors, ^{9}Be breakup.]

I. INTRODUCTION

Single-neutron stripping reactions induced by heavy ions such as ^{7}Li, ^{11}B, ^{12}C, ^{14}N, and ^{16}O at bombarding energies not too far above the Coulomb barrier have been investigated extensively over the past few years.[1-8] These reactions all involve the transfer of a neutron that is fairly tightly bound in the projectile (by 7.2–18.7 MeV). Thus, the ground-state reaction Q values are generally negative and transitions to high-spin states at low excitation energies are favored. The only heavy-ion projectile with a substantially smaller neutron-separation energy is ^{9}Be(S_n = 1.67 MeV), which is even more weakly bound than the deuteron (S_n = 2.22 MeV). Since the Q values for the (^{9}Be, ^{8}Be) reaction are typically positive, the (^{9}Be, ^{8}Be) reaction is expected to favor transitions that are kinematically inhibited in other heavy-ion reactions, namely, those involving small angular momentum transfers at high excitation energies, and these transitions should be well described by standard distorted-wave Born-approximation (DWBA) calculations.

On the other hand, the small separation energy of ^{9}Be can also give rise to a breakup process $^9\text{Be} \rightarrow {}^8\text{Be} + n$ in the field of the target nucleus, similar to that observed for the deuteron, $d \rightarrow p + n$. If the magnitude of this process is large, the coupling of the breakup to the direct transfer channel may be important and could lead to a breakdown of the conventional DWBA model.

The (^{9}Be, ^{8}Be) reaction has been studied only recently[9] because of problems[10] in the acceleration of ^{9}Be (due to the absence of gaseous compounds of beryllium and the high toxicity of beryllium compounds) and difficulties in detecting the particle-unbound ^{8}Be. Nevertheless, this reaction has experimental advantages over other heavy-ion single-neutron transfer reactions. A ^{8}Be detection system[11] is capable of eliminating both (a) the excited states of the outgoing particle (^{8}Be*) from the energy spectra and (b) the more copiously produced elastically and inelastically scattered beam particles; both of these can be sources of spurious peaks in heavy-ion single-neutron transfer reactions.

In the present work we report energy spectra for the (^{9}Be, ^{8}Be) reaction on ^{12}C, ^{16}O, ^{26}Mg, ^{28}Si, ^{40}Ca, and ^{208}Pb targets at a bombarding energy of 50 MeV. For the ^{28}Si, ^{40}Ca, and ^{208}Pb targets, angular distributions were measured and analyzed in terms of the exact finite-range DWBA using optical model potentials obtained by fitting the measured ^{9}Be elastic-scattering data.

II. EXPERIMENTAL METHOD

The experiments discussed in his work utilized a 50-MeV $^9\text{Be}^{2+}$ beam from the Lawrence Berkeley Laboratory 88-inch cyclotron at intensities of up to 100 nA on target. The $^9\text{Be}^{2+}$ ions were produced in a Penning Ion Gauge source[12] to which argon was added to sputter beryllium atoms from a piece

of beryllium metal into the arc where they were ionized. This technique was used in place of the more common method of mixing the source material (lithium, boron) into the cathode buttons in order to reduce the safety problems associated with the handling of the highly toxic beryllium.

The detection of ^{8}Be(g.s.) nuclei[13] is complicated by the fact that they decay promptly ($\tau \sim 10^{-16}$ s), and must be observed indirectly be means of their decay α particles. The decay of the ^{8}Be ground state is characterized by a single decay channel, a small decay energy (92 keV), two identical charged products and, since all the spins involved are zero, an isotropic distribution of the decay products in their center of mass. For relatively high-energy ^{8}Be events [$E(^8\text{Be}) > 35$ MeV], the decay α particles are kinematically focused into a narrow cone (apex angle $<6°$) whose axis lies in the direction of the original ^{8}Be event. Since the decay energy is small compared to the ^{8}Be energy, the two α particles have approximately equal energies and velocities. Therefore, they will reach a detection system almost simultaneously and a ^{8}Be event can be characterized by detecting both particles in coincidence.

Because the distribution of the α particles is sharply peaked at the surface of the breakup cone, a large solid angle is required to detect both α particles with high efficiency, whereas a small horizontal acceptance angle is required for good energy resolution. If a position-sensitive detector (PSD) is placed behind a twin transmission ΔE detector[13] (see Fig. 1), it is possible to measure both the direction and energy of a ^{8}Be event; with this approach the detection efficiency and the energy resolution can be optimized concurrently. Since the two α particles strike the PSD at nearly equal distances from the axis of the breakup cone, the average position signal X corresponds to the direction of the original ^{8}Be event (see Fig. 1). Thus one can compensate kinematic broadening by gating the energy signals with position signals corresponding to a small angular range. To further characterize ^{8}Be events, particle identification is performed using the summed ΔE signals and the E signal from the PSD (^{8}Be identifies[13] as if it were a ^{7}Li event). Because they have considerably larger breakup cones, decay products from excited states of ^{8}Be are not detected by this system (see Refs. 11 and 13 for a more detailed discussion of the ^{8}Be identifier).

To study the (^{9}Be, ^{8}Be) reaction, a ^{8}Be identifier with a large effective solid angle was utilized which consisted of 100-μm phosphorus-diffused silicon twin transmission detectors (10×13 mm^2) and a 300-μm surface-barrier silicon PSD (10×30 mm^2). Because of the large horizontal acceptance angle (9°), three position gates were set on the ^{8}Be energy spectra. Each gate was 1.4° wide and subtended an effective solid angle of 0.35 msr with a calculated detection efficiency[14] of about 18%. The observed energy resolution of 450 keV full width at

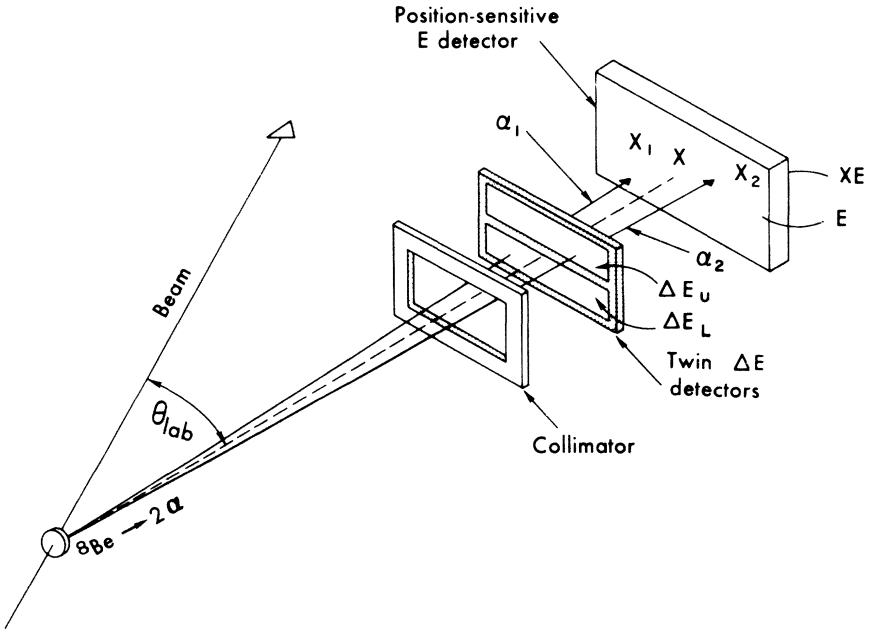

FIG. 1. Schematic diagram of the ^{8}Be identifier showing twin transmission detectors, PSD, trajectories of the breakup α particles (solid lines), and measured direction of the ^{8}Be event (dashed line).

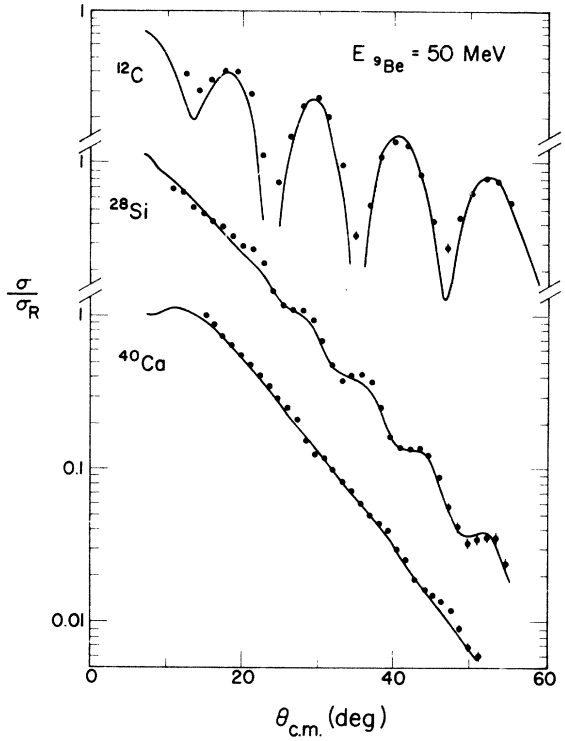

FIG. 2. Elastic-scattering angular distributions (plotted as a ratio to Rutherford cross section) for 50-MeV ^{9}Be on targets of ^{12}C, ^{28}Si, and ^{40}Ca. The solid lines are optical-model calculations using the potentials in Table I.

half maximum was mainly determined by the kinematic broadening. With this system a singles count rate of 15 000 s^{-1} in each ΔE detector could be maintained with an associated dead time of less than 20%.

In the same experiment, ^{9}Be elastic scattering was measured utilizing a 300-μm silicon surface-barrier PSD with a width of 50 mm and a height of 10 mm. A collimator was employed which consisted of a tantalum plate with eight vertical slits (10×1 mm^2) separated by 2 mm. The energy signal was routed by the corresponding position signal; thus elastic scattering was simultaneously measured at eight angles, each with a horizontal acceptance of 0.5° and separated by 1°.

III. ELASTIC-SCATTERING DATA

Elastic scattering of ^{9}Be at 50 MeV from ^{12}C, ^{28}Si, and ^{40}Ca targets was measured between 10° and 60° and from a ^{208}Pb target between 60° and 100° in the center of mass. The angular distributions are shown in Figs. 2 and 3 as the ratio of the elastic to Rutherford cross sections. Only statistical error bars are indicated; the absolute cross sections are expected to be accurate to ±15%. For

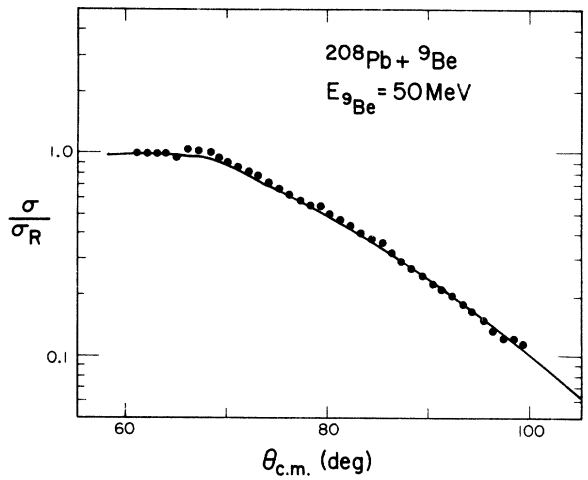

FIG. 3. Elastic scattering angular distribution (plotted as a ratio to Rutherford cross section) for 50-MeV ^{9}Be on ^{208}Pb. The solid line is an optical-model calculation using the potential in Table I.

the light target, ^{12}C, the distribution is strongly oscillatory (Fraunhofer-type scattering), while with increasing atomic number, and thus increasing Coulomb field, the oscillations weaken (^{28}Si) and then disappear (^{208}Pb, Fresnel-type scattering).[15]

Figures 2 and 3 also show fits obtained from optical-model calculations using a modified version of the search code GENOA.[16] For the nuclear part of the potential, only real and imaginary volume terms of Woods-Saxon form were included and for the Coulomb part a spherical charge distribution with radius $1.2(A_P^{1/3}+A_T^{1/3})$ fm was taken. The potential parameters extracted from a six-parameter search and used in the distorted-wave Born-approximation (DWBA) calculations are listed in Table I.

IV. REACTION DATA

Heavy-ion reactions show a pronounced dependence of the yield on the reaction kinematics, which is discussed in Sec. IV A in view of the particular kinematic conditions which result from

TABLE I. Optical-model parameters.

Target	V (MeV)	r_{0R} [a] (fm)	a_R (fm)	W (MeV)	r_{0I} [a] (fm)	a_I (fm)
^{12}C	85.3	1.01	0.64	23.9	0.94	0.89
^{28}Si	72.0	1.05	0.61	11.2	1.30	0.85
^{40}Ca	65.4	0.86	0.79	10.1	1.28	0.80
^{208}Pb	61.9	1.26	0.40	3.37	1.32	0.92

[a] $R = r_0 (A_P^{1/3} + A_T^{1/3})$.

employing the weakly bound projectile ^{9}Be. In Sec. IV B the single-particle states observed in the energy spectra of the (^{9}Be, ^{8}Be) reaction on ^{12}C, ^{16}O, ^{26}Mg, ^{28}Si, ^{40}Ca, and ^{208}Pb targets are discussed in detail; angular distributions and a DWBA analysis are presented in Sec. IV C. Finally, the broad continuum that is seen in the energy spectra is treated in Sec. IV D.

A. Kinematical effects

There are two main kinematical factors that determine the yield of heavy-ion reactions: the Q value and the angular momentum matching. At energies above the Coulomb barrier, semiclassical considerations by Brink[17,3] show that, in the reaction $A(a,b)B$, the probability for transferring a nucleon, or a cluster of nucleons, with mass m is highest for transitions with Q values around a perferred Q value, Q_p, which is given by

$$Q_p = -\tfrac{1}{2}mv^2 + \frac{(Z_bZ_B - Z_aZ_A)e^2}{R}, \tag{1}$$

where v is the relative velocity of the projectile and target nuclei in the region of transfer, Z is the atomic number, and $R = r_0(a^{1/3} + A^{1/3})$, the distance at the point of interaction. The first term in Eq. (1) can be calculated from the following expression:

$$\tfrac{1}{2}\mu v^2 = E_{\text{c.m.}} - U, \tag{2}$$

where μ and $E_{\text{c.m.}}$ are, respectively, the entrance channel reduced mass and the center-of-mass energy and $U = Z_aZ_Ae^2/R$ is the Coulomb potential energy at the distance R. Using Eq. (2) and noting that the second term in Eq. (1) vanishes for neutron-transfer reactions, one finds

$$Q_p = -\frac{m}{\mu}(E_{\text{c.m.}} - U). \tag{3}$$

The preferred excitation energy E_p in the residual nucleus is then given by

$$E_p = Q_0 - Q_p, \tag{4}$$

where Q_0 is the ground-state Q value. Table II presents the values of Q_0, Q_p, and E_p, calculated using $r_0 = 1.4$ fm, for the (^{9}Be, ^{8}Be) reaction at 50 MeV on the targets investigated in this work. At this bombarding energy, E_p is typically between 7 and 10 MeV; the smaller value for ^{208}Pb is caused by the large Coulomb potential energy. These E_p values are quite high, even though the bombarding energy is relatively low, due to the positive Q_0 values associated with the small neutron-separation energy of ^{9}Be. For comparison, these quantities have also been calculated for two other heavy-ion neutron-transfer reactions with projectiles of comparable mass and which have been studied at a similar energy per nucleon: (^{7}Li, ^{6}Li) at 36 MeV (Ref. 1) and (^{11}B, ^{10}B) at 72 MeV (Ref. 4). Whereas the Q_p values for these three reactions are roughly the same, the E_p values for the latter two reactions are significantly lower due to their smaller Q_0 values. Higher values of E_p for the ^{7}Li and ^{11}B induced reactions can only be achieved at much higher bombarding energies.

The other kinematical factor is the angular momentum matching[18] between the initial and final orbits for a surface reaction. The yield is large if the orbital angular momentum transfer l fulfills the matching condition:

$$l \approx \Delta L = |L_{0i} - L_{0f}|, \tag{5}$$

where L_{0i} and L_{0f} are the partial waves in the initial and the final channels for which the amplitude of the elastic S matrix is equal to 0.5. For a given reaction, ΔL depends strongly on the Q value of the transition and somewhat less on the bombarding energy. For the (^{9}Be, ^{8}Be) reaction at 50 MeV, values of ΔL have been determined for a light (^{12}C), medium (^{40}Ca), and heavy (^{208}Pb) target from optical-model calculations using the parameters listed in Table I for both the entrance and exit

TABLE II. Ground-state Q value, Q_0; theoretical preferred Q value, Q_p[Eq. (3)]; and excitation energy, E_p [Eq. (4)] for the (^{9}Be, ^{8}Be) reaction at 50 MeV compared with the values for the (^{7}Li, ^{6}Li) reaction at 36 MeV and the (^{11}B, ^{10}B) reaction at 72 MeV.

	(^{9}Be, ^{8}Be) 50 MeV			(^{7}Li, ^{6}Li) 36 MeV			(^{11}B, ^{10}B) 72 MeV		
Target	Q_0 (MeV)	Q_p (MeV)	E_p (MeV)	Q_0 (MeV)	Q_p (MeV)	E_p (MeV)	Q_0 (MeV)	Q_p (MeV)	E_p (MeV)
^{12}C	3.28	−4.5	7.8	−2.31	−4.2	1.9	−6.51	−5.4	−1.1
^{16}O	2.48	−4.3	6.8	−3.11	−4.0	0.9	−7.31	−5.3	−2.0
^{26}Mg	4.77	−4.1	8.9	−0.81	−3.8	3.0	−5.02	−5.1	0.1
^{28}Si	6.81	−3.9	10.7	1.22	−3.6	4.8	−2.98	−4.9	1.9
^{40}Ca	6.68	−3.5	10.2	1.10	−3.2	4.3	−3.11	−4.5	1.4
^{208}Pb	2.28	−0.7	3.0	−3.31	−0.4	−2.9	−7.51	−1.6	−5.9

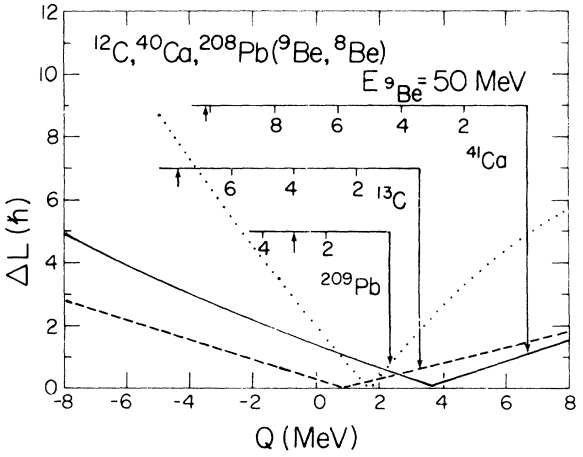

FIG. 4. Plot of ΔL vs Q value for the (^{9}Be, ^{8}Be) reaction on ^{12}C (dashed line), ^{40}Ca (solid line), and ^{208}Pb (dotted line) targets at 50 MeV. Ground-state Q values and an excitation energy scale are given for each final nucleus, and the preferred excitation energies are indicated by upward-pointing arrows.

channels; these are plotted as a function of the Q value in Fig. 4. At this bombarding energy, ΔL is zero for Q values around 2 MeV and increases almost linearly for larger and smaller values with a slope that steepens with increasing target mass. Also indicated in Fig. 4 are the ground-state Q values (Q_0), excitation energy scales for the region in which the single-particle states lie, and the preferred excitation energy E_p taken from Table II. In general, the Q_0 values fall on the right (more positive Q value) side of the minimum in the ΔL curves and the corresponding ΔL values are around $1\hbar$. Then, for transitions to excited states, ΔL first decreases but, after going through zero, increases to a value of about $2-3\hbar$ for excitation energies near E_p. For excitation energies below E_p, optimum angular momentum matching is therefore achieved for small l transfers, that is for transitions to low-spin states; transitions involving large l transfers are kinematically inhibited. This is quite different from the conditions encountered in other heavy-ion single-neutron transfer reactions with similar mass projectiles at comparable incident energies. Since these other reactions all have less positive Q_0 values than the (^{9}Be, ^{8}Be) reaction, their Q_0 values lie on the left side of the minimum in the ΔL curves and therefore ΔL increases monotonically for transitions to excited states, resulting in an angular momentum mismatch for small l transfers.

Based on Q_p and ΔL, Brink has also derived more detailed formulas[3,17] for predicting the relative transition probabilities in heavy-ion reactions. They have been tested for the present reaction using the computer code HIPROB.[19] However, it was found that the observed preferential population of the low-spin states was not predicted correctly. That is, for transitions with $\Delta L \approx 0$ and $l \gg \Delta L$, the angular momentum mismatch did not result in a reduction of the calculated transition probabilities. On the other hand, for those reactions in which large angular momentum transfers are favored [$\Delta L \gg 0$, e.g., ^{208}Pb(^{11}B, ^{10}B)^{209}Pb] and for which the model has been successfully applied[3] so far, the calculations clearly show a smaller probability for transitions that have $l \approx 0$.

B. Energy spectra

In the following subsections, the single-particle states observed in energy spectra from the (^{9}Be, ^{8}Be) reaction will be discussed and contrasted with results from other heavy-ion single-neutron stripping reactions where available. Errors on excitation energies of peaks which cannot be assigned to known states are typically ±100 keV.

1. $^{12}C(^{9}Be,^{8}Be)^{13}C$

In the energy spectrum shown in Fig 5(a), transitions are observed to the known[20] single-particle states in ^{13}C with the following energies and configurations: ground-state, $1p_{1/2}$; 3.09 MeV, $2s_{1/2}$; 3.85 MeV, $1d_{5/2}$; and 8.2 MeV, $1d_{3/2}$. Furthermore, the 6.86-MeV, $\frac{5}{2}^{+}$ state and levels at 7.5, 9.5, and 10.8 MeV are weakly populated; the last three levels cannot be uniquely identified with known states. The fact that states at these high excitation energies are populated is due to the large value of E_p (7.8 MeV). In other heavy-ion reactions such as the (^{7}Li, ^{6}Li) reaction[1] at 36 MeV, these states are only very weakly excited because E_p is small (1.9 MeV). On the other hand, at much higher incident energies, the (^{11}B, ^{10}B) and the (^{12}C, ^{11}C) reactions[3] at 114 MeV as well the (^{14}N, ^{13}N) reaction[7] at 155 MeV populate states up to about 11 MeV, very much like the (^{9}Be, ^{8}Be) reaction, since at these energies the E_p values of the reactions approach that of the (^{9}Be, ^{8}Be) reaction at 50-MeV bombarding energy.

2. $^{16}O(^{9}Be,^{8}Be)^{17}O$

Figure 5(b) presents an energy spectrum from the (^{9}Be, ^{8}Be) reaction on a SiO_2 target. The preferred excitation energy for this reaction on ^{16}O is 6.8 MeV; thus the following states which are known[21] to have substantial single-particle character are populated: ground state, $1d_{5/2}$; 0.87 MeV, $2s_{1/2}$; 5.08 MeV, $1d_{3/2}$; and 5.70 MeV, $1f_{7/2}$. A strong transition is also observed to a state at 7.6 MeV with a possible $2p_{3/2}$ configuration.[21] The

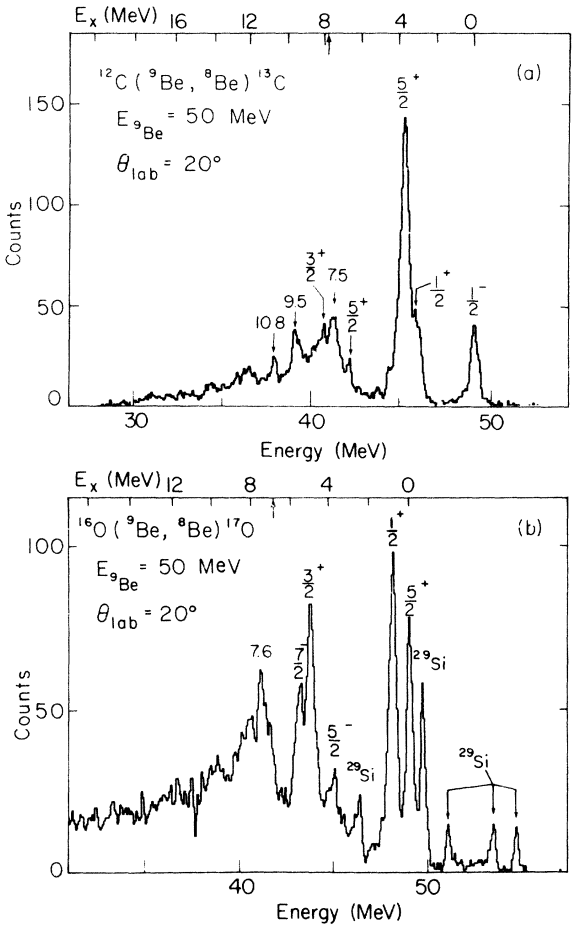

FIG. 5. ^{8}Be energy spectra from (a) the ^{12}C(^{9}Be, ^{8}Be) ^{13}C and (b) the ^{16}O(^{9}Be, ^{8}Be)^{17}O reactions (the latter using an SiO_2 target). The population of known final states is denoted with the appropriate J^π values; transitions which cannot be uniquely identified are labeled with excitation energies. The arrows on the upper excitation energy scales indicate the calculated values of E_p.

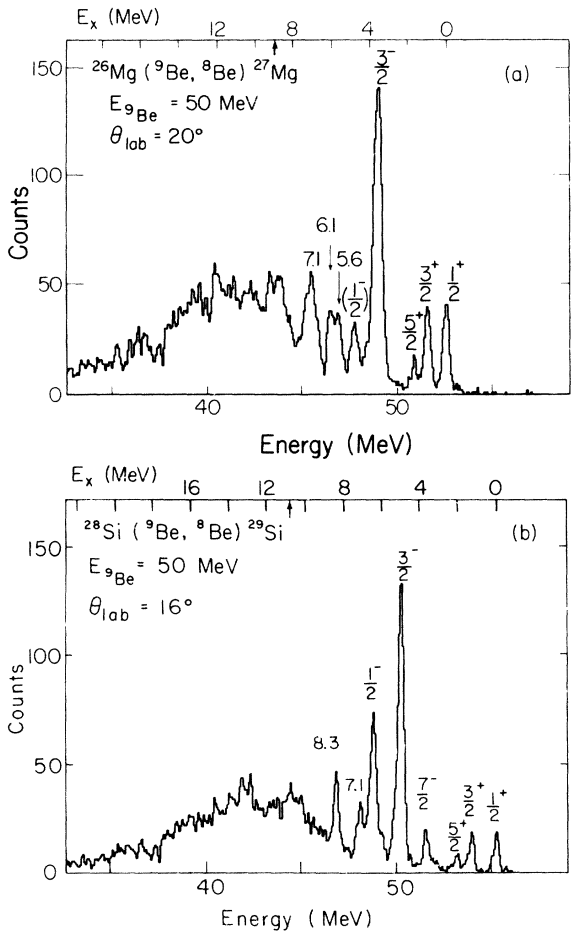

FIG. 6. ^{8}Be energy spectra from (a) the ^{26}Mg(^{9}Be, ^{8}Be) ^{27}Mg and (b) the ^{28}Si(^{9}Be, ^{8}Be)^{29}Si reactions. See caption to Fig. 5.

$\frac{5}{2}^-$ state at 3.84 MeV is only weakly populated; this is similar to results from the ^{16}O(d, p)^{17}O reaction[22] where it was found that this $\frac{5}{2}^-$ state was not populated in a simple stripping reaction. In contrast to these ^{16}O(^{9}Be, ^{8}Be)^{17}O data, the (^{7}Li, ^{6}Li) reaction[1] at 36 MeV (E_p = 0.9 MeV) predominantly excites the ^{17}O ground state with a decreasing yield to excited states.

3. ^{26}Mg(^{9}Be,^{8}Be)^{27}Mg and ^{28}Si(^{9}Be,^{8}Be)^{29}Si

Since ^{26}Mg and ^{28}Si have the same number of neutrons, the energy spectra from the (^{9}Be, ^{8}Be) reaction on these two targets are expected to be quite similar. Spectra from the two reactions are shown in Figs. 6(a) and 6(b) at θ_{lab} = 20° and 16°, respectively. Known[23] states with single-particle configuration $2s_{1/2}$, $1d_{3/2}$, $1d_{5/2}$, and $2p_{3/2}$ at 0.0, 0.98, 1.70, and 3.56 MeV in ^{27}Mg and at 0.0, 1.27, 2.03, and 4.93 MeV in ^{29}Si are in fact populated with the same relative strengths. The $1f_{7/2}$ level, which is only weakly populated in ^{29}Si at 3.62 MeV, lies in ^{27}Mg above the $2p_{3/2}$ level by 200 keV and could not be resolved. A state observed in ^{27}Mg at 4.8 MeV with a tentative assignment of ($\frac{1}{2}^-$, $\frac{3}{2}^-$) (Ref. 23) could correspond to the known[23] 6.38-MeV $\frac{1}{2}^-$ level in ^{29}Si.

Because the (^{9}Be, ^{8}Be) reaction on both the ^{26}Mg and ^{28}Si targets has a high preferred excitation energy (8.9 and 10.7 MeV, respectively), states in ^{27}Mg and ^{29}Si are appreciably populated up to 8 MeV. At the higher excitation energies the density of states increases, making an identification of the observed peaks with known states difficult. In ^{27}Mg two (poorly resolved) peaks at 5.6 and 6.1 MeV as well as a broad peak at 7.1 MeV are populated, while in ^{29}Si peaks at 7.1 and 8.3 MeV are

observed.

In contrast to these data from the (^{9}Be, ^{8}Be) reaction on ^{26}Mg and ^{28}Si, other single-neutron stripping reactions at a comparable bombarding energy[1] (36-MeV ^{7}Li) or at higher energies[5,8] (114-MeV ^{11}B and 126-MeV ^{16}O) populate states at lower excitation energies (<4 MeV) because their more negative Q values shift downward the preferred excitation energy (see Table II) and also increase ΔL. Thus, for the (^{7}Li, ^{6}Li) reaction[1] on ^{28}Si, the strongest transition is observed to the $1d_{3/2}$, 1.27-MeV state which is only moderately populated by the (^{9}Be, ^{8}Be) reaction. Furthermore, the large ΔL values for the (^{11}B, ^{10}B) and (^{16}O, ^{15}O) reactions[5,8] on ^{26}Mg cause them to populate strongly the high-spin state with configuration $1f_{7/2}$ at 3.76 MeV in ^{27}Mg; this state is unresolved in the (^{9}Be, ^{8}Be) data but, based on the observed excitation energy of the peak corresponding to the $\frac{3}{2}^-$, 3.56-MeV state, is only weakly excited.

4. $^{40}Ca(^9Be,^8Be)^{41}Ca$

Figure 7(a) presents an energy spectrum from the (^{9}Be, ^{8}Be) reaction on ^{40}Ca. Transitions are observed to the $1f_{7/2}$ ground state, two states with a substantial $2p_{3/2}$ configuration at 1.94 and 2.46 MeV and two states with an appreciable $2p_{1/2}$ configuration at 3.94 and 4.75 MeV.[23] The state at 5.6 MeV, the broad (possibly a doublet) state at 7.5 MeV and a sharp state at 8.6 MeV, which is above the neutron threshold of 8.4 MeV, cannot be identified with particular known levels.

As can be seen from Fig. 4, one has $\Delta L < 1$ for transitions to states in ^{41}Ca with excitation energies below 5 MeV. Since orbital angular momentum transfer values of 2, 3, or 4 are required for the transition to the $\frac{7}{2}^-$, ground state of ^{41}Ca, the angular momentum mismatch results in a smaller cross section than for the transitions with good angular momentum matching such as those to the first two $\frac{3}{2}^-$ and $\frac{1}{2}^-$ states, where a neutron is deposited in a p orbital with possible l transfers of 0 (for the $\frac{3}{2}^-$ states), 1, or 2.

5. $^{208}Pb(^9Be,^8Be)^{209}Pb$

A typical energy spectrum of the ^{208}Pb(^{9}Be, ^{8}Be)-^{209}Pb reaction is presented in Fig. 7(b). Transitions to the following reasonably pure single-particle states[24] are observed: ground state, $2g_{9/2}$; 0.78 MeV, $1i_{11/2}$; 1.57 MeV, $3d_{5/2}$; and 2.54 MeV, $3d_{3/2}$. The 1.42-MeV, $1j_{15/2}$; 2.03-MeV, $4s_{1/2}$; and 2.49-MeV, $2g_{7/2}$ states are not resolved from the two strongly populated states at 1.57 MeV, $\frac{5}{2}^+$ and 2.54 MeV, $\frac{3}{2}^+$.

The data in Fig. 7(b) clearly show a substantial decrease in yield for the high-spin states relative

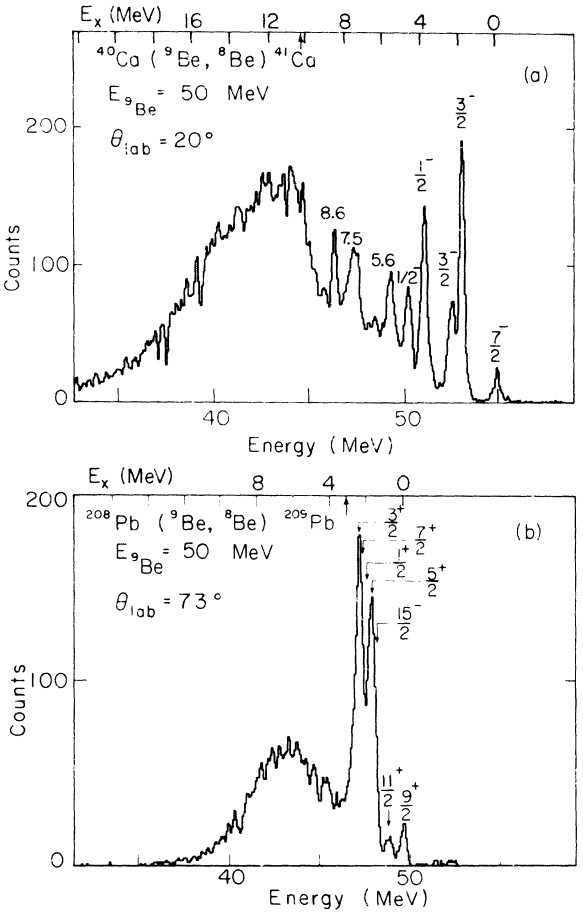

FIG. 7. ^{8}Be energy spectra from (a) the ^{40}Ca(^{9}Be, ^{8}Be)^{41}Ca and (b) the ^{208}Pb(^{9}Be, ^{8}Be)^{209}Pb reactions. See caption to Fig. 5.

to that for the lower-spin states. Since the single-particle spectroscopic strengths for all these states are close to unity, the differences in population are entirely due to a kinematical effect, namely, the angular momentum mismatch discussed in Sec. IV A. For the transitions to the $\frac{9}{2}^+$, ground state and the first excited state, $\frac{11}{2}^+$, $\Delta L < 1\hbar$ (see Fig. 4), whereas the allowed l-transfer values are 3, 4, 5 and 5, 6, 7, respectively, giving rise to a substantial mismatch. For the transitions to low-spin states ($\frac{5}{2}^+$, $\frac{1}{2}^+$, and $\frac{3}{2}^+$) around 2-MeV excitation, both the l matching and the Q matching ($E_p = 3$ MeV) are good. This accounts for the large observed cross sections to these states.

The kinematic behavior of the (^{9}Be, ^{8}Be) reaction differs strikingly from similar heavy-ion reactions, such as the (^{11}B, ^{10}B) reaction[4] at 72 MeV, in which the ΔL value is around $10\hbar$ for the ground state transition and becomes even larger for transitions to excited states. Thus there is a large

angular momentum mismatch for all transitions except those involving very large angular momentum transfers, and as a result only high-spin states were observed (with decreasing cross sections for the excited states since $E_p = -5.9$ MeV). A similar comment applies to the ^{208}Pb(^{11}B, ^{10}B) reaction[2] at 113.5 MeV and the ^{208}Pb(^{16}O, ^{15}O) reaction[6] at 139 MeV where only the high-spin states were observed.

C. Angular distributions

For the (^{9}Be, ^{8}Be) reaction on ^{28}Si, ^{40}Ca, and ^{208}Pb targets, angular distributions for transitions to states with known spin and parity are presented in Figs. 8–10. The angular distributions for the ^{28}Si target show some diffraction structure (see Fig. 8) while those observed for ^{40}Ca and ^{208}Pb are almost featureless (see Figs. 9 and 10), as is typical of low energy heavy-ion reactions. [The distribution for the unresolved 2.03-MeV, $\frac{1}{2}^+$ state in ^{209}Pb (Fig. 10) was obtained by a multiple peak fitting analysis.] Only statistical error bars are shown; the uncertainty in the absolute cross sections is about ±25%.

These angular distributions were analyzed in terms of exact finite-range DWBA using the computer code PTOLEMY,[25] which calculates the differential cross section by

$$\frac{d\sigma}{d\Omega} = \sum_l S_B S_{^9\mathrm{Be}} \sigma^l_{\mathrm{DWBA}}, \qquad (6)$$

where S_B and $S_{^9\mathrm{Be}}$ are the single-neutron spectroscopic factors for the residual nucleus and the projectile, respectively. The contributions from all allowed l transfers were added incoherently since in the calculation of the distorted waves no spin-orbit interaction was used.

Optical-model parameters, derived from ^{9}Be elastic scattering (Table I) were used for both the entrance and exit channels. This approximation should not be unreasonable since both ^{9}Be

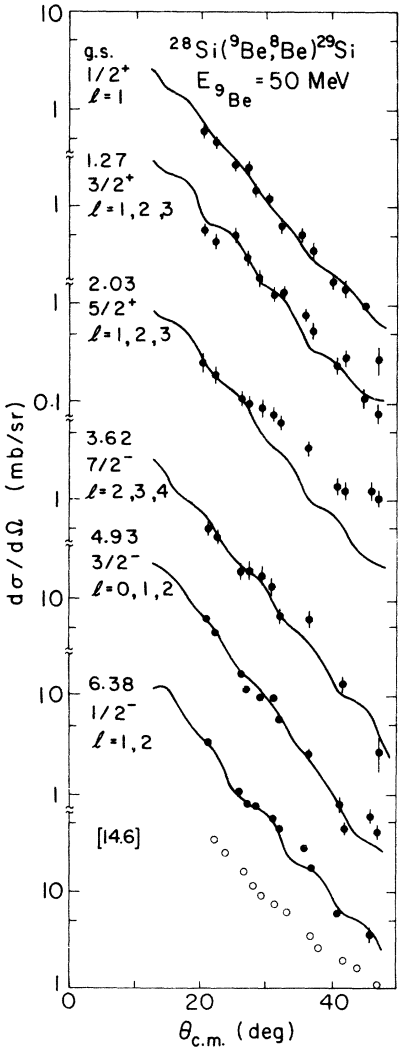

FIG. 8. Angular distributions for transitions to single-particle states (dots) and the continuum (open circles) for the ^{28}Si(^{9}Be, ^{8}Be)^{29}Si reaction. Only statistical error bars are shown. The solid lines represent DWBA calculations using the optical potential in Table I and normalized with the spectroscopic factors given in Table III.

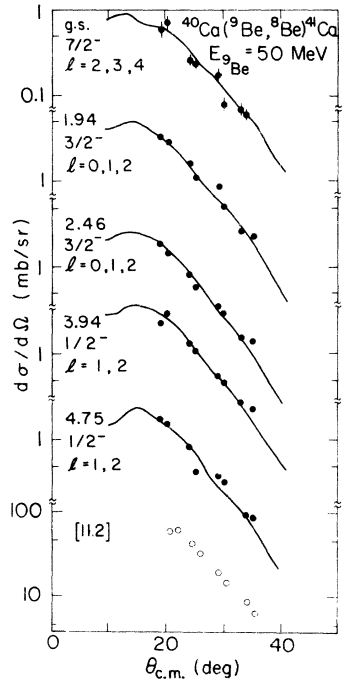

FIG. 9. Angular distributions for transitions to single-particle states (dots) and the continuum (open circles) for the ^{40}Ca(^{9}Be, ^{8}Be)^{41}Ca reaction. See caption to Figure 8.

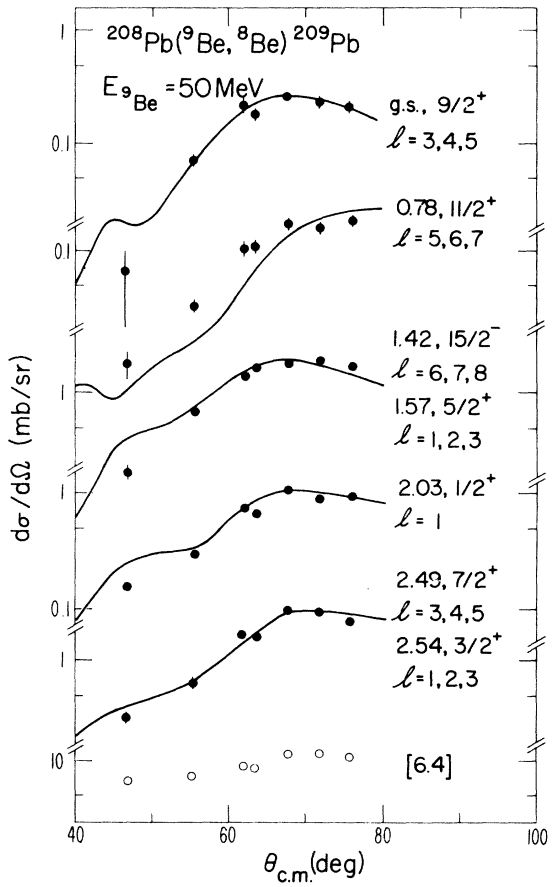

FIG. 10. Angular distributions for transitions to single-particle states (dots) and the continuum (open circles) for the ^{208}Pb(^{9}Be, ^{8}Be)^{209}Pb reaction. See caption to Figure 8.

and ^{8}Be are weakly bound structures of similar mass and identical charge. The bound-state wave functions were determined using a real Woods-Saxon potential with radius $R_{b.s.} = 1.25 \times A^{1/3}$ fm, diffuseness $a = 0.65$ fm, and a spin-orbit strength $V_{s.o.} = 6$ MeV. The depth of the potential well was adjusted to give the neutron separation energy.

The results of the calculations are shown in Figs. 8–10. In general the shapes of the distributions are well reproduced by the theory. Extracted absolute and relative spectroscopic factors S_B are given in Table III where for $S_{^{9}Be}$ the theoretical value[26] of 0.58 was used. Although the relative spectroscopic factors are in fairly good agreement with those obtained from light-ion reactions,[27-29] the absolute values for all the targets are too small; i.e., the magnitude of the predicted cross section is too large by an average factor of 1.3, 3.3, and 5.2 for ^{28}Si, ^{40}Ca, and ^{208}Pb, respectively.

Several effects could account for this discrepancy in the absolute magnitudes of spectroscopic factors. There is, of course, an uncertainty in the optical potential for the exit channel since no elastic-scattering data exist. For the ^{40}Ca and ^{208}Pb targets, where the cross sections were overestimated the most by the DWBA, different optical-potential parameter sets that fitted the elastic scattering equally well were tried; however, neither the shape nor the magnitude of the predicted cross section was very sensitive to these parameters, so long as they fitted the elastic-scattering data. Furthermore, a variation of the bound state radius $R_{b.s.}$ did not affect the magnitude of the calculated cross sections significantly. It is possible, however, that the overestimation of the cross section arises from the fact that the strong observed breakup of ^{9}Be (see Sec. IV D) was not properly accounted for in these calculations. Although in conventional DWBA such effects are implicitly contained in the absorptive part of the optical potential, coupling of the breakup channel to the transfer channel and the distortion of the internal wave function of the projectile, which are likely to be important in the presence of a strong breakup process, are neglected. Attempts[30,31] to improve the DWBA calculations by including breakup of the projectile have mainly concentrated on the analysis of deuteron stripping reactions. Perhaps the simplest and most successful approach is that of Johnson and Soper.[30] Their theory leads

TABLE III. Absolute and relative spectroscopic factors.

Final nucleus	E_x (MeV)	nl_j	(^{9}Be, ^{8}Be) S_{abs}	(^{9}Be, ^{8}Be) S_{rel}	(d,p) [a] S_{abs}	(d,p) [a] S_{rel}
^{29}Si	g.s	$2s_{1/2}$	0.31	1	0.53	1
	1.27	$1d_{3/2}$	0.61	1.97	0.74	1.40
	2.03	$1d_{5/2}$	0.09	0.29	0.12	0.23
	3.62	$1f_{7/2}$	0.25	0.81	0.38	0.58
	4.93	$2p_{3/2}$	0.49	1.55	0.56	1.06
	6.38	$2p_{1/2}$	0.49	1.55	0.53	1.00
^{41}Ca	g.s.	$1f_{7/2}$	0.21	1	0.95	1
	1.94	$2p_{3/2}$	0.20	0.95	0.70	1.36
	2.46	$2p_{3/2}$	0.08	0.38	0.25	0.36
	3.94	$2p_{1/2}$	0.18	0.86	0.67	0.96
	4.75	$2p_{1/2}$	0.10	0.48	0.19	0.27
^{209}Pb	g.s.	$2g_{9/2}$	0.16	1	0.83	1
	0.78	$1i_{11/2}$	0.24	1.50	0.86	1.04
	1.42	$1j_{15/2}$	0.19 [b]	1.19	0.58	0.70
	1.57	$3d_{5/2}$			0.98	1.18
	2.03	$4s_{1/2}$	0.14	0.88	0.98	1.18
	2.49	$2g_{7/2}$	0.17 [b]	1.06	1.05	1.27
	2.54	$3d_{3/2}$			1.07	1.29

[a] Ref. 27 for ^{29}Si, Ref. 28 for ^{41}Ca, and Ref. 29 for ^{209}Pb.

[b] Average value obtained by dividing the experimental cross section for these unresolved states by the sum of the calculated cross sections.

to a stripping matrix element similar to that in the DWBA, except that the deuteron optical potential is replaced by an effective potential—the adiabatic potential—which is derived from phenomenological neutron and proton optical potentials. To date this model has not been applied to heavy-ion reactions. Although the (^{9}Be, ^{8}Be) reaction seems to be particularly well suited for studies of breakup effects in heavy-ion reactions, the application of the adiabatic theory is complicated by the unbound nature of ^{8}Be (since optical potentials for this particle-unstable nuclide would be required).

D. ^{9}Be breakup

In all the ^{8}Be energy spectra, particularly those for the heavier targets ^{40}Ca and ^{208}Pb (Fig. 7), a rather large, roughly Gaussian-shaped continuum was observed. This continuum is peaked close to the preferred excitation energy E_p in the final nucleus. On the other hand, if expressed in terms of the ^{8}Be energy, the centroid of the distribution for all the targets is around 43 MeV which corresponds to a ^{8}Be velocity equal to that of the ^{9}Be projectile reduced somewhat by the neutron separation energy of ^{9}Be. Thus, the yield for this continuum could come from two reaction mechanisms: direct neutron transfer to a region having a high density of states with single-particle strength, or "quasielastic" breakup of $^9\mathrm{Be} \rightarrow {}^8\mathrm{Be} + n$. Because of the small neutron separation energy of ^{9}Be, and the fact that this structure appears with each target, the latter process is likely to be dominant. Breakup of the ^{9}Be projectile has been observed previously at beam energies both below and above the Coulomb barrier. Sub-Coulomb breakup of ^{9}Be on gold has been measured by Lang *et al.*[32] and analyzed with semiclassical calculations. At energies above the Coulomb barrier, evidence for the breakup of the ^{9}Be projectile has been obtained in the (^{9}Be, α) reaction,[10] in which the α-particle energy spectra exhibited a large background which was ascribed to the two-step disintegration $^9\mathrm{Be} \rightarrow {}^8\mathrm{Be} + n$ followed by $^8\mathrm{Be} \rightarrow 2\alpha$ as well as three-body processes such as $^9\mathrm{Be} \rightarrow 2\alpha + n$.

Under the assumption that the continuum observed in the (^{9}Be, ^{8}Be) reaction is entirely due to breakup, rough differential cross sections were extracted from the various energy spectra and the angular distributions are shown in the lower portion of Figs. 8–10. The slopes of these distributions are about the same as for the single-particle transitions—rising towards the grazing angle (see Fig. 10) and falling behind it (see Figs. 8 and 9)—as expected for a quasielastic process. For the ^{208}Pb target, the distribution is somewhat flatter compared to those observed for discrete transitions (see Fig. 10), which could indicate that breakup is significant even at larger impact parameters. The peak cross sections for breakup on the ^{28}Si, ^{40}Ca, and ^{208}Pb targets are about 30, 60, and 10 mb/sr, respectively. It is somewhat surprising that the breakup cross section for ^{208}Pb is smaller than that for ^{28}Si and ^{40}Ca. However, similar results have been observed in a study[33] of the dissociation of ^{6}Li into $\alpha + d$, where it was found that, at a bombarding energy of 36 MeV, the breakup cross section on Ni was smaller than on ^{12}C.

V. SUMMARY

It has been shown that the unusually small neutron-separation energy of ^{9}Be gives rise to kinematical conditions that distinguish the (^{9}Be, ^{8}Be) reaction from other one-neutron stripping reactions induced by heavy ions at low bombarding energies. This reaction populates low-spin states up to several MeV in excitation with considerable strength, whereas most other heavy ion reactions, due to their more negative Q values, preferentially populate higher-spin states at low excitation energies. In addition, evidence for a considerable projectile breakup process was obtained in the form of a large continuum in the ^{8}Be energy spectra. Even though exact finite-range DWBA predicts the shapes of the angular distributions and the relative cross sections for the single-particle transitions correctly, it overestimates the absolute magnitude, especially for the heavier targets. It is believed that this disagreement may be caused by the strong projectile breakup process not taken into account by the conventional DWBA theory.

We wish to thank Dr. D. K. Scott for many helpful discussions and for a critical reading of the manuscript, as well as J. Bowen and the cyclotron crew for developing the beryllium beam.

---

†Work performed under the auspices of the U. S. Energy Research and Development Administration.

*Present address: Michigan State University, East Lansing, Michigan 48824.

[1]P. Schumacher, N. Ueta, H. D. Duhm, K. I.-Kubo, and W. J. Klages, Nucl. Phys. A212, 573 (1973).

[2]A. Anyas-Weiss, J. Becker, T. A. Belote, J. C. Cornell, P. S. Fisher, P. N. Hudson, A. Menchaca-Rocha, A. D. Panagiotou, and D. K. Scott, Phys. Lett. 45B, 231 (1973).

[3]N. Anyas-Weiss, J. C. Cornell, P. S. Fisher, P. N. Hudson, A. Menchaca-Rocha, D. J. Millener, A. D.

Panagiotou, D. K. Scott, D. Strottman, D. M. Brink, B. Buck, P. J. Ellis, and T. England, Phys. Rep. 12C, 201 (1974).
[4]J. L. C. Ford, Jr., K. S. Toth, G. R. Satchler, D. C. Hensley, L. W. Owen, R. M. DeVries, R. M. Gaedke, P. J. Riley, and S. T. Thornton, Phys. Rev. C 10, 1429 (1974).
[5]I. Paschopoulos, P. S. Fisher, N. A. Jelley, S. Kahana, A. A. Pilt, W. D. M. Rae, and D. Sinclair, Nucl. Phys. A252, 173 (1975).
[6]F. D. Becchetti, B. G. Harvey, D. Kovar, J. Mahoney, C. Maguire, and D. K. Scott, Phys. Rev. C 12, 894 (1975).
[7]K. G. Nair, H. Voit, C. W. Towsley, M. Hamm, J. D. Bronson, and K. Nagatani, Phys. Rev. C 12, 1575 (1975).
[8]D. Sinclair, I. Paschopoulos, H. S. Bradlow, P. S. Fisher, A. A. Pilt, and W. D. M. Rae, Nucl. Phys. A261, 511 (1976).
[9]J. Lang, R. Müller, J. Unternährer, L. Jarezyk, B. Kamys, and A. Strzalkowski, in Proceedings of European Conference on Nuclear Physics with Heavy Ions, Caen, 1976 (unpublished), p. 39.
[10]N. I. Venikov, Yu. A. Glukhov, V. I. Man'kov, B. G. Novatskii, A. A. Ogloblin, S. B. Sakuta, D. N. Stepanov, V. N. Unezhev, V. I. Chuev, and N. I. Chumakov, Yad. Fiz. 22, 924 (1975) [Sov. J. Nucl. Phys. 22, 481 (1976)].
[11]G. J. Wozniak, D. P. Stahel, J. Cerny, and N. A. Jelley, Phys. Rev. C 14, 815 (1976).
[12]D. J. Clark, J. Steyaert, J. Bowen, A. Carneiro, and D. Morris, in *Proceedings of the 6th International Cyclotron Conference, Vancouver, 1972,* edited by J. J. Burgerjon and A. Strathdee (AIP, New York, 1972), p. 265.
[13]G. J. Wozniak, N. A. Jelley, and J. Cerny, Nucl. Instrum. Methods 120, 29 (1974).
[14]Copies of the program EFFCR are available from the authors upon request.
[15]W. E. Frahn, Phys. Rev. Lett. 26, 568 (1971).
[16]F. G. Perey, optical-model search code GENOA (unpublished).
[17]D. M. Brink, Phys. Lett. 40B, 37 (1972).
[18]R. Stock, R. Bock, P. David, H. H. Duhm, and T. Tamura, Nucl. Phys. A104, 136 (1967).
[19]Computer code HIPROB, provided by Dr. P. N. Hudson, Oxford University, Oxford, England.
[20]F. Ajzenberg-Selove, Nucl. Phys. A268, 1 (1976).
[21]F. Ajzenberg-Selove, Nucl. Phys. A281, 1 (1977).
[22]S. E. Darden, S. Sen, H. R. Hiddleston, J. A. Aymar, and W. A. Yoh, Nucl. Phys. A208, 77 (1973).
[23]P. M. Endt and C. van der Leun, Nucl. Phys. A214, 1 (1973).
[24]M. J. Martin, Nucl. Data B6, 287 (1971).
[25]D. H. Gloeckner, M. H. Macfarlane, and S. C. Pieper, Argonne National Laboratory Report No. ANL-76-11 (unpublished).
[26]S. Cohen and D. Kurath, Nucl. Phys. 101, 1 (1967).
[27]M. C. Mermaz, C. A. Whitten, Jr., J. W. Champlin, A. J. Howard, and D. A. Bromley, Phys. Rev. C 4, 1778 (1971).
[28]D. C. Kocher and W. Haeberli, Nucl. Phys. A196, 225 (1972).
[29]D. G. Kovar, N. Stein, and C. K. Bockelman, Nucl. Phys. A231, 266 (1974).
[30]R. C. Johnson and P. J. R. Soper, Phys. Rev. C 1, 976 (1970).
[31]J. P. Farrell, Jr., C. M. Vincent, and N. Austern, Ann. Phys. (N.Y.) 96, 333 (1976).
[32]J. Lang, R. Müller, E. Ungricht, and J. Unternährer, in Proceedings of the European Conference on Nuclear Physics with Heavy Ions, Caen, 1976 (unpublished), p. 48.
[33]R. W. Ollerhead, C. Chasman, and D. A. Bromley, Phys. Rev. 134, B74 (1964).